



EDGE ARTICLE

Cite this: *Chem. Sci.*, 2021, 12, 15691

All publication charges for this article have been paid for by the Royal Society of Chemistry

Second-sphere effects on H₂O₂ activation by non-heme Fe^{II} complexes: role of a phenol group in the [H₂O₂]-dependent accumulation of Fe^{IV}O vs. Fe^{III}OOH†

Jean-Noël Rebilly,* Christian Herrero, Katell Sénéchal-David, Régis Guillot,  Tanya Inceoglu, Hélène Maisonneuve and Frédéric Banse *

Redox metalloenzymes achieve very selective oxidation reactions under mild conditions using O₂ or H₂O₂ as oxidants and release harmless side-products like water. Their oxidation selectivity is intrinsically linked to the control of the oxidizing species generated during the catalytic cycle. To do so, a second coordination sphere is used in order to create a pull effect during the activation of O₂ or H₂O₂, thus ensuring a heterolytic O–O bond cleavage. Herein, we report the synthesis and study of a new non-heme Fe^{II} complex bearing a pentaazadentate first coordination sphere and a pendant phenol group. Its reaction with H₂O₂ generates the classical Fe^{III}OOH species at high H₂O₂ loading. But at low H₂O₂ concentrations, an Fe^{IV}O species is generated instead. The formation of the latter is directly related to the presence of the 2nd sphere phenol group. Kinetic, variable temperature and labelling studies support the involvement of the attached phenol as a second coordination sphere moiety (weak acid) during H₂O₂ activation. Our results suggest a direct Fe^{II} → Fe^{IV}O conversion directed by the 2nd sphere phenol via the protonation of the distal O atom of the Fe^{II}/H₂O₂ adduct leading to a heterolytic O–O bond cleavage.

Received 18th June 2021
Accepted 17th November 2021

DOI: 10.1039/d1sc03303d

rsc.li/chemical-science

Introduction

Redox metalloenzymes carry out oxidation reactions at room temperature with high efficiency.¹ In cytochrome P450 or Rieske dioxygenases, O₂ is activated by sequential electron and proton transfers from a reductase to generate the active species: a (P⁺) Fe^{IV}O species in cytochrome P450 (“compound I”)^{2–7} and a proposed *cis* Fe^V(O)(OH) or Fe^{IV}(O)(OH) species in the case of Rieske dioxygenases.^{8–13} In both cases, an Fe^{III}OOH intermediate is the precursor that results from O₂ reductive activation. Such an intermediate can be generated with non-heme iron complexes using the peroxide shunt pathway^{14–17} and was demonstrated to be involved in oxidation reactions.^{14,18,19} Usually, when non-heme Fe^{II} complexes are used as precursors, they react in a two-step process: (i) Fe^{II} is oxidized by a 1st equivalent of H₂O₂ through a homolytic process to yield a {Fe^{III}OH; HO•} pair, with HO• readily reacting with either the solvent²⁰ or another Fe^{II} complex²¹ and (ii) the resulting Fe^{III}OH is involved in a substitution reaction with a 2nd equivalent of H₂O₂ to yield Fe^{III}OOH.^{21–25} The H₂O₂ activation pathway can be modulated by taking inspiration from natural

systems. In peroxidases and catalases, a heterolytic activation of H₂O₂ is observed in a single step (Fe^{III} to formally Fe^VO). To achieve this, a histidine, assisted by an arginine or asparagine residue in the 2nd sphere²⁶ shuttles the proton of Fe^{III}-bound H₂O₂ from the proximal to the distal O atom in order to polarize the O–O bond, create a pull effect and ensure the heterolytic cleavage of the O–O bond.^{5,6,27} In peroxidases, a water molecule located between the histidine and the Fe^{III}-H₂O₂ moiety further facilitates the proton transfer by reinforcing the H-bond network.²⁸

Inspired by this strategy, we report here a new non-heme Fe^{II} complex based on a pentaazadentate coordination sphere incorporating a phenol group in the 2nd coordination sphere. Remarkably, a switch in the H₂O₂ activation mechanism is observed depending on reaction conditions: at high H₂O₂ loading, the classical Fe^{III}(OOH) species is formed, while Fe^{IV}O is predominantly accumulated at low H₂O₂ concentration. We demonstrate by thorough kinetic studies that the latter forms faster than Fe^{III}(OOH), and that Fe^{IV}O forms from Fe^{II} through the heterolytic activation of an Fe^{II}/H₂O₂ adduct assisted by the 2nd sphere acidic phenol.

Results and discussion

Ligand synthesis

L₅^{PhOH} (Chart 1) was synthesized from **mpL**₄² (Scheme S2†) and 2,4-di-*tert*-butyl-6-(azidomethyl)phenol by the CuAAC

Université Paris-Saclay, CNRS, Institut de Chimie Moléculaire et des Matériaux d'Orsay (ICMMO), 91405 Orsay Cedex, France. E-mail: jean-noël.rebilly@universite-paris-saclay.fr; frederic.banse@universite-paris-saclay.fr

† Electronic supplementary information (ESI) available. CCDC 1992915 and 1992916. For ESI and crystallographic data in CIF or other electronic format see DOI: 10.1039/d1sc03303d



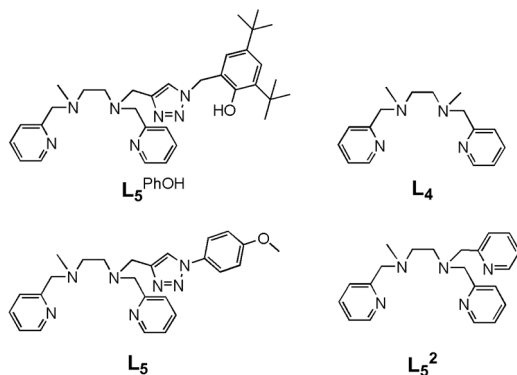


Chart 1 Structure of the ligands mentioned in this paper.

methodology using CuSO_4 /sodium ascorbate in *t*BuOH/water in 67% yield (Schemes S1–S3 and Fig. S1–S6†).

Synthesis of the complexes

The complete experimental procedures are described in the ESI.†

$[(\text{L}_5^{\text{PhOH}})\text{Fe}^{\text{II}}\text{Cl}_2]$ (1) was obtained in quantitative yield by filtration of the yellow precipitate that appears after 3 days in MeCN upon mixing equimolar quantities of L_5^{PhOH} and $\text{Fe}^{\text{II}}\text{Cl}_2$.

$[(\text{L}_5^{\text{PhOH}})\text{Fe}^{\text{II}}\text{Cl}](\text{PF}_6)$ (2) was isolated in 71% yield after addition of 1 equiv. AgPF_6 to $[(\text{L}_5^{\text{PhOH}})\text{Fe}^{\text{II}}\text{Cl}_2]$ in MeCN and removal of AgCl .

$[(\text{L}_5^{\text{PhOH}})\text{Fe}^{\text{II}}(\text{MeCN})](\text{PF}_6)_2$ (3) was obtained in 74% yield after reaction of two equiv. AgPF_6 with $[(\text{L}_5^{\text{PhOH}})\text{Fe}^{\text{II}}\text{Cl}_2]$ in MeCN. $[(\text{L}_5^{\text{PhOH}})\text{Fe}^{\text{II}}(\text{OTf})](\text{OTf})$ (4) was prepared from L_5^{PhOH} and $\text{Fe}^{\text{II}}(\text{OTf})_2$ in MeCN and isolated in 82% yield.

All complexes were characterized by UV-vis spectroscopy, cyclic voltammetry (CV) and ESI-MS (Fig. S7–S21†).

Solid state studies

Single crystals of $[(\text{L}_5^{\text{PhOH}})\text{Fe}^{\text{II}}\text{Cl}](\text{PF}_6)$ (2) were obtained by slow diffusion of *t*BuOMe into a methanolic solution of the complex. The same procedure applied to complex (3) led to single crystals of a rearranged complex of formula $[(\text{L}_5^{\text{PhOH}})\text{Fe}^{\text{II}}(\text{H}_2\text{O})(\text{OH})](\text{PF}_6)$ (5).

The crystal structure of the molecular cation $[(\text{L}_5^{\text{PhOH}})\text{FeCl}]^+$ of (2) (Fig. 1a) shows a distorted octahedral environment and an overall binding mode very similar to that of the parent complex $[(\text{L}_5)\text{FeCl}](\text{PF}_6)$.²⁰ L_5^{PhOH} acts as a pentadentate ligand with its two pyridines sitting in *trans* positions. The 6th position is occupied by the chloride ion. With bond distances between 2.17 and 2.30 Å, the complex is in line with structural data reported for high spin Fe^{II} centers, which is expected with a bound anion.²⁹ In this structure, the distance between the phenol oxygen and the metal center is 6.49 Å.

$[(\text{L}_5^{\text{PhOH}})\text{Fe}^{\text{II}}(\text{H}_2\text{O})(\text{OH})](\text{PF}_6)$ (5) shows a different binding mode (Fig. 1b). The metal sits in a pseudo-octahedral environment, but L_5^{PhOH} now acts as a tetradentate ligand. The two pyridines still occupy *trans* positions, but in this case neither the triazole nor the phenol group are bound to the metal. The

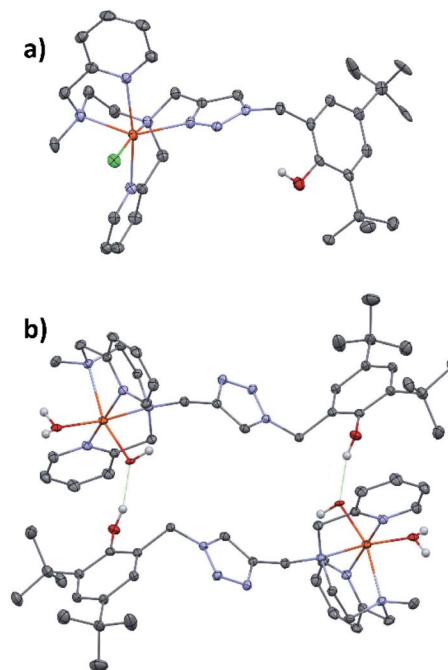


Fig. 1 ORTEP drawing of compounds (a) $[(\text{L}_5^{\text{PhOH}})\text{Fe}^{\text{II}}\text{Cl}]^+$ of (2) and (b) $[(\text{L}_5^{\text{PhOH}})\text{Fe}^{\text{II}}(\text{H}_2\text{O})(\text{OH})]^+$ of (5). Thermal ellipsoids are shown at the 30% level. Fe is in orange-red, C in grey, N in blue, O in dark red, Cl in green.

coordination sphere is completed by an aquo and an hydroxo ligands. Bond distances lie in the range 2.10–2.22 Å (Fe–N) and 1.86–1.88 Å (Fe–O). In the unit cell, this structure is stabilized by intermolecular hydrogen bonds developing within supramolecular dimers: the hydroxo ligand of one complex is hydrogen-bonded to the dangling phenol group of the partner in a head-to-tail fashion.

$[(\text{L}_5^{\text{PhOH}})\text{Fe}^{\text{II}}(\text{H}_2\text{O})(\text{OH})](\text{PF}_6)$ (5) could not be isolated in pure form in bulk quantities. Therefore, it was not studied in solution but its structure is mentioned here to support the triazole lability discussed later.

In the following reactivity and spectroscopic studies, we will only focus on the triflate salt $[(\text{L}_5^{\text{PhOH}})\text{Fe}^{\text{II}}(\text{OTf})](\text{OTf})$ (4), as triflate, unlike chloride, is readily displaced by MeCN in the coordination sphere of iron.²⁹

Solution studies

The CV (Fig. S20†) of $[(\text{L}_5^{\text{PhOH}})\text{Fe}^{\text{II}}(\text{OTf})](\text{OTf})$ (4) in MeCN indicates a major $[(\text{N}_5)\text{Fe}^{\text{II}}(\text{MeCN})]^{2+}$ species ($E_p^a = 1.0$ V), and a very minor $[(\text{N}_5)\text{Fe}^{\text{II}}(\text{OTf})]^+$ one ($E_p^a = 0.69$ V), identified by analogy with parents complexes, and confirming that triflate is easily substituted by MeCN.^{20,29} The triazole functional group is bound to the metal while the phenol group is free in the 2nd coordination sphere, as evidenced by its oxidation wave at $E_p^a = 1.61$ V.³⁰ Furthermore, a reduction wave ascribed to the reduction of the phenolic proton is observed at $E_p^c = -1.55$ V. Accordingly, the $\text{Fe}^{\text{II}} \rightarrow \text{py}$ MLCT observed at 379 nm ($\epsilon = 4400$ L mol⁻¹ cm⁻¹) (Fig. S19†) shows a magnitude that is significantly higher than that of $[(\text{L}_5^{\text{PhOH}})\text{Fe}^{\text{II}}\text{Cl}](\text{PF}_6)$ (2)

(385 nm, $\epsilon = 1100 \text{ L mol}^{-1} \text{ cm}^{-1}$). This is indicative of more covalent Fe^{II}-py bonds in **4**, in agreement with a more pronounced low spin character. This is confirmed by magnetic moment determination by NMR in solution (Evans method, Fig. S22†). While **2** displays a high spin ($S = 2$) state ($\mu_{\text{eff}} = 5.06 \mu_{\text{B}}$), **4** displays a μ_{eff} of $3.3 \mu_{\text{B}}$, which indicates a spin state equilibrium between a high spin ($S = 2$) and low spin ($S = 0$) species. The same value of μ_{eff} is found for **3** which points toward the substitution of the anionic triflate by MeCN. This spectroscopic signature is typical of $[(\text{N}_5)\text{Fe}^{\text{II}}(\text{MeCN})]^{2+}$ complexes in solution.^{20,29} Compound **4** in solution adopts a similar binding mode as $[(\text{L}_5^{\text{PhOH}})\text{Fe}^{\text{II}}\text{Cl}](\text{PF}_6)$, with the stronger field MeCN as exogenous ligand instead of Cl⁻.

Spectroscopic studies of intermediates

Generation and decay of Fe^{IV}O species generated with iodosylbenzene. Single oxygen atom donors are frequently used to prepare Fe^{IV}O species from Fe^{II} complexes in a direct reaction. Therefore, they are convenient reactants to follow the generation and fate of reaction intermediates. The possibility to stabilize reactive species from **4** and the impact of the second sphere phenol on its stability were first assessed using iodosylbenzene.

Iodosylbenzene (1.3 equiv. dissolved in MeOH/MeCN 1 : 15) was added to a 1 mM solution of **4** in MeCN at 293 K and the evolution of the UV-vis spectrum was followed using a stopped flow spectrophotometer (Fig. 2 and S23†). Between 0 and 0.7 s (Fig. 2a), the tail of the Fe^{II} → py MLCT (379 nm) decreases, indicating oxidation of Fe^{II}, together with the growth of a new band at 736 nm, characteristic of an Fe^{IV}O species.^{20,29,31,32} Based on the extinction coefficient of parent complex $[(\text{L}_5^2)\text{Fe}^{\text{IV}}\text{O}]^{2+}$ ($\epsilon = 300 \text{ L mol}^{-1} \text{ cm}^{-1}$),³³ a conversion of Fe^{II} to Fe^{IV}O of 86% can be estimated. The intermediate then decays to yield a new chromophore at 627 nm, typical of a PhO⁻ → Fe^{III} LMCT (Fig. 2b and c).³⁴ The Fe^{IV}O decay is better fitted to a 2nd order kinetics, which indicates a bimolecular decay process (Fig. S24†). The EPR spectrum recorded at 90 K of a solution frozen in liquid nitrogen just after mixing reactants in the tube displays a main signal in the HS region ($g = 8.55, 4.3$) expected for Fe^{III}(OPh)³⁴ and non-specific (rhombic) high spin species (Fig. S25†). In the low spin region, two species are detected with parameters $g = 2.320, 2.170, 1.935$ and $g = 2.320, 2.145, 1.935$, which can be ascribed to $(\text{N}_5)\text{Fe}^{\text{III}}(\text{OMe})^{2+}$ and $(\text{N}_4)\text{Fe}^{\text{III}}(\text{OMe})(\text{MeCN})^{2+}$,^{29,35–37} together with a radical signal at $g = 2.004$ (Fig. 2d).

The formation and decay of $[(\text{L}_5^{\text{PhOH}})\text{Fe}^{\text{IV}}\text{O}]^{2+}$ (and its analogue without the phenol group $[(\text{L}_5)\text{Fe}^{\text{IV}}\text{O}]^{2+}$) can be followed by ESI-MS. The time evolution of the mass spectrum with the $(\text{L}_5^{\text{PhOH}})$ complex shows the decay of the starting Fe^{II} complex to yield Fe^{III} complexes, with the transient formation of Fe^{IV}O within a 10 s window in line with the half-life determined by UV-vis spectroscopy (Fig. S28–S31†). Interestingly, unlike the case of the (L_5) complex (Fig. S32 and S33†) where the peaks correspond to a single ion, the peaks of Fe^{IV} and Fe^{III} species with $(\text{L}_5^{\text{PhOH}})$ are split (Fig. S29–S31†). The features can be nicely simulated as the superimposition of the isotopic patterns

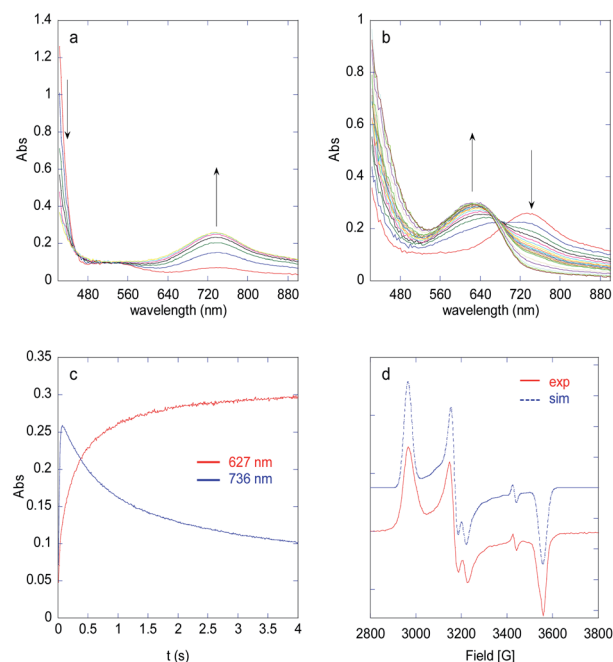
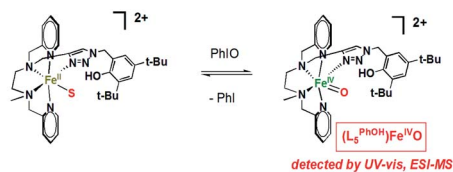
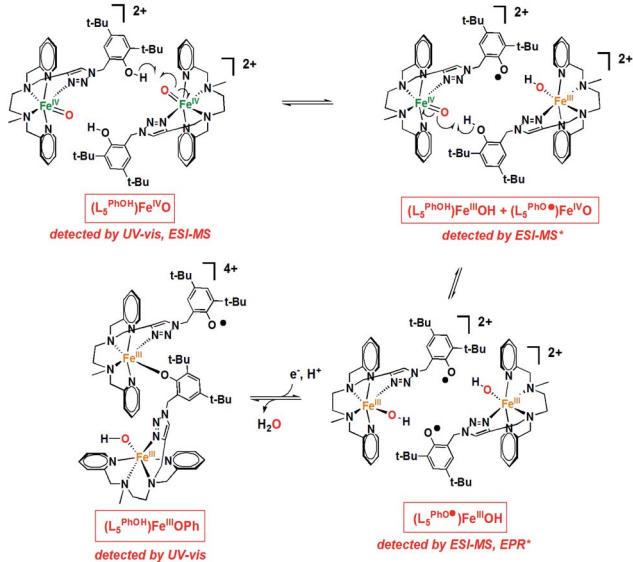


Fig. 2 Evolution of the UV-vis spectrum of a 1 mM solution of $[(\text{L}_5^{\text{PhOH}})\text{Fe}^{\text{II}}(\text{OTf})](\text{OTf})$ (**4**) in MeCN upon addition of 1.3 equiv. PhIO at 293 K: growth of the Fe^{IV}O species (a) and its decay to yield a Fe^{III}(OPh) species (b). Time traces at 627 and 736 nm (c). X band EPR spectrum in MeCN (90 K) of a mixture of $[(\text{L}_5^{\text{PhOH}})\text{Fe}^{\text{II}}(\text{OTf})](\text{OTf})$ (**4**) in MeCN and 1.2 equiv. PhIO and simulated spectrum as the sum of 3 components (d) (component A: $g = 2.320, 2.170, 1.935$; component B: $g = 2.320, 2.145, 1.935$; radical: $g = 2.004$ in a A/B ratio of 1/0.4). These LS signals represent 25% of the initial Fe^{II}.

of $(\text{L}_5^{\text{PhOH}})\text{Fe}$ and $(\text{L}_5^{\text{PhO}^\cdot})\text{Fe}$ species, where $\text{L}_5^{\text{PhO}^\cdot}$ results from phenol H atom abstraction by an oxidizing species.

All these observations can be rationalized by the mechanism proposed in Scheme 1. O-atom transfer from PhIO to Fe^{II} generates an Fe^{IV}O intermediate, which is capable of electron and proton abstraction from the 2nd sphere phenol. Indeed, $[(\text{L}_5^{\text{PhOH}})\text{Fe}^{\text{IV}}\text{O}]^{2+}$ decays with a half-life $t_{1/2} = 3.9 \text{ s}$ vs. $t_{1/2} = 34.8 \text{ s}$ for $[(\text{L}_5)\text{Fe}^{\text{IV}}\text{O}]^{2+}$ deprived of phenol (Fig. S23†). The 2nd order decay of the intermediate suggests a bimolecular process, which is in line with the geometric constraints of the complex (the phenol moiety can only engage in intermolecular interactions with a metal center). This reaction between the metal and the phenol yields Fe^{III}(OH), readily converted to Fe^{III}(OMe) in the presence of MeOH, and a phenoxyl radical on the neighboring complex, which are both detected by EPR (Fig. 2 and S25–S27†) and ESI-MS (Fig. S28, S30, and S31†). In these conditions, the radical is reduced quickly to phenolate (by remaining Fe^{II}, or by oxidation of the solvent or an oxidizable site of the bound ligand) which undergoes further stabilisation as an intermolecular Fe^{III}(OPh) species detected by UV-vis spectroscopy. The time evolution of the radical is detailed in Fig. S26, S27, and Scheme S4.† For the sake of simplicity, we represent the decay product as a dimeric structure but it could be another oligomeric form (Scheme 1). Interestingly, reactivity studies provide further support to the proposed mechanism: the reaction of **4** with 2 equiv. PhIO and cyclooctene (800 equiv.)

Formation of $\text{Fe}^{\text{IV}}\text{O}$ Intermolecular decay of $\text{Fe}^{\text{IV}}\text{O}$ 

Scheme 1 Proposed mechanism for the growth and decay of the $\text{Fe}^{\text{IV}}\text{O}$ species generated with iododisylbenzene. S stands for MeCN. Note (*): the $\text{Fe}^{\text{III}}(\text{OH})$ species indicated in this scheme are readily displaced in the presence of MeOH towards their $\text{Fe}^{\text{III}}(\text{OMe})$ counterparts (detected by EPR and ESI-MS). For clarity, these equilibria are omitted here.

yields cyclooctene oxide, confirming the formation of a reactive species capable of epoxidation. Furthermore, the yield is decreased by 27% when compared to the same reaction carried out with $[(\text{L}_5)\text{Fe}^{\text{II}}(\text{OTf})](\text{OTf})$, not bearing the 2nd sphere phenol group, in line with the interception of $\text{Fe}^{\text{IV}}\text{O}$ by the phenol (Table S1†).

Generation of $\text{Fe}^{\text{III}}(\text{OOH})$ at high H_2O_2 loading. In order to evaluate the impact of the 2nd sphere phenol group on H_2O_2 activation, we performed studies in the conditions commonly used to accumulate the $\text{Fe}^{\text{III}}(\text{OOH})$ intermediate, *e.g.* using an excess of H_2O_2 . Upon addition of 100 equiv. H_2O_2 to a 1 mM solution of **4** in MeCN at 293 K, the UV-vis spectrum shows a decrease of the $\text{Fe}^{\text{II}} \rightarrow \text{py}$ MLCT along with the growth of a new band at 529 nm, ascribed to the formation of a $\text{Fe}^{\text{III}}(\text{OOH})$ species (Fig. 3a).^{14,29,36,38–40} Based on the extinction coefficient of the parent $[(\text{L}_5)\text{Fe}^{\text{III}}(\text{OOH})]^{2+}$ ($\epsilon = 760 \text{ L mol}^{-1} \text{ cm}^{-1}$),²⁰ bearing the same 1st coordination sphere, the maximum accumulation corresponds to a 90% conversion of Fe^{II} to $\text{Fe}^{\text{III}}(\text{OOH})$. The chromophore then decays within *ca.* 10 minutes (Fig. S35†). The conversion into $\text{Fe}^{\text{III}}(\text{OOH})$ as well as the time needed for its decay are dependent on $[\text{H}_2\text{O}_2]$ (Fig. S36†). This is typical of the steady-state generation of such intermediates which also react with the oxidant, as frequently observed.^{33,41} The nature of the

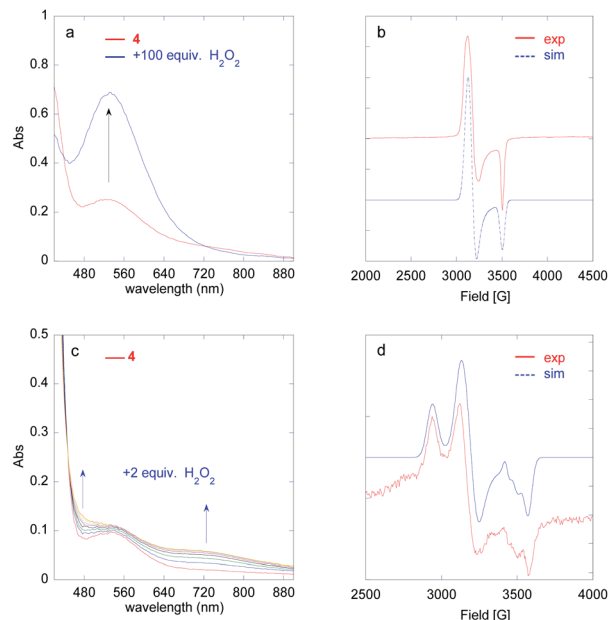
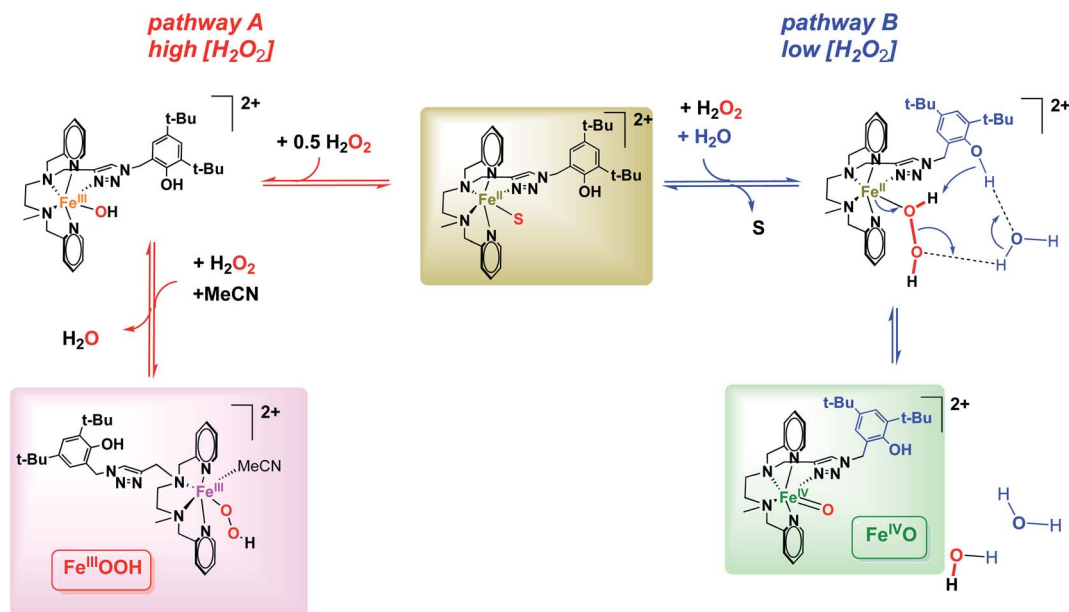


Fig. 3 Generation of $\text{Fe}^{\text{III}}(\text{OOH})$ (a) and $\text{Fe}^{\text{IV}}\text{O}$ (c) species followed by UV-vis spectroscopy upon addition of 100 equiv. (a) or 2 equiv. (c) H_2O_2 to a 1 mM solution of $[(\text{L}_5^{\text{PhOH}})\text{Fe}^{\text{II}}(\text{OTf})](\text{OTf})$ (**4**) in MeCN at 293 K. X band EPR spectrum in MeCN (90 K) of the solution drawn at the maximum of the 530 nm band ((b), 100 equiv. H_2O_2) and at the maximum of the 730 nm band ((d), 2 equiv. H_2O_2). Experimental spectrum (red) and simulation (blue) with $g = 2.205, 2.165, 1.965$. (b). Experimental spectrum (red) and simulation (blue) as a sum of 3 components. The LS signals are residual and only represent 7% of the initial Fe^{II} (d): component A ($\text{Fe}^{\text{III}}(\text{OH})$): $g = 2.340, 2.140, 1.928$; component B ($(\text{N}_4)\text{Fe}^{\text{III}}(\text{OOH})(\text{MeCN})^{2+}$): $g = 2.205, 2.165, 1.965$; radical: $g = 2.004$.

intermediate was confirmed by EPR spectroscopy of a sample frozen after the addition of 100 equiv. H_2O_2 to a 2 mM solution of (**4**) in MeCN at 293 K (Fig. 3b and S37†). The spectrum displays a low spin signal, with $g = 2.205, 2.165, 1.965$, which resembles the one of documented non-heme $\text{Fe}^{\text{III}}(\text{OOH})$ intermediates.^{35,36} Interestingly, it is very similar to that observed with $[(\text{L}_5)\text{Fe}^{\text{III}}(\text{OTf})](\text{OTf})$, which was identified as a $\text{Fe}^{\text{III}}(\text{OOH})$ species bound in a tetradentate fashion (triazole is unbound, Scheme 2, pathway A).²⁰

The growth of $\text{Fe}^{\text{III}}(\text{OOH})$ was fitted at 530 nm using a mono-exponential kinetics law. The rate constant for the formation of $\text{Fe}^{\text{III}}(\text{OOH})$ shows a linear dependence on H_2O_2 concentration (Fig. S38†), in line with a bimolecular reaction between the iron complex and the oxidant as previously observed for the parent $[(\text{L}_5)\text{Fe}^{\text{III}}(\text{OOH})]^{2+}$ species.²⁰

Generation of $\text{Fe}^{\text{IV}}\text{O}$ at low H_2O_2 loading. The complex **4** seems to display a classical behavior at high H_2O_2 loading, but excess H_2O_2 can be a potential scavenger for a transient reaction intermediate such as $\text{Fe}^{\text{III}}(\text{OOH})$ or $\text{Fe}^{\text{IV}}\text{O}$.^{33,41,42} We thus decreased the amount of oxidant to near stoichiometric conditions in order to unravel the role of the 2nd sphere phenol. Interestingly, when H_2O_2 concentration is lowered, the UV-vis spectrum shows an additional chromophore around 730 nm (Fig. S35†). For 2 equiv. H_2O_2 , the 730 nm chromophore becomes predominant (Fig. 3c). This is ascribed to the



Scheme 2 Proposed mechanisms for the activation of H₂O₂ to Fe^{III}(OOH) (pathway A) and Fe^{IV}O species (pathways B), depending on H₂O₂ concentration. S stands for MeCN.

formation of a Fe^{IV}O species (*vide supra*), which is confirmed by HR-ESI-MS experiments (Fig. 4 and S39–S41†).

The spectrum obtained upon mixing 2 eq. H₂O₂ with the Fe^{II} complex in MeCN is dominated by a massif around $m/z = 760$ corresponding to the starting $[(L_5^{\text{PhOH}})\text{Fe}^{\text{II}}(\text{OTf})]^+$ ion and its oxidized form $[(L_5^{\text{PhO}^\cdot})\text{Fe}^{\text{II}}(\text{OTf})]^+$. But a second massif around $m/z = 776$ corresponds to the overlay of three ions: $[(L_5^{\text{PhOH}})\text{Fe}^{\text{IV}}(\text{O})(\text{OTf})]^+$, its oxidized form $[(L_5^{\text{PhO}^\cdot})\text{Fe}^{\text{IV}}(\text{O})(\text{OTf})]^+$ and its decay product $[(L_5^{\text{PhOH}})\text{Fe}^{\text{III}}(\text{OH})(\text{OTf})]^+$ (Fig. S40 and S41†), confirming the formation of the Fe^{IV}O intermediate. When the reaction is carried out using H₂¹⁸O₂, a similar massif is obtained, but with an increased intensity of the peak at $m/z = 778.2549$ corresponding to the insertion of ¹⁸O (Fig. S42 and S43†). This confirms that the oxo species results from the activation of H₂O₂.

In order to get more insight into the formation of the Fe^{IV}O species, the evolution of Fe^{IV}O absorption was fitted at 730 nm using a biexponential A → B → C law describing its formation and its subsequent decay (Fig. S44†).

The formation rate of the Fe^{IV}O species shows a linear dependence on [H₂O₂] (Fig. S44†). This is in line with a bimolecular process between the Fe^{II} complex and H₂O₂. Furthermore, Fe^{IV}O forms much faster than Fe^{III}(OOH). Indeed, the observed rate constant for the formation of Fe^{IV}O ($k_{1\text{obs}}$ (730 nm)) is nearly 5 times that of Fe^{III}(OOH) ($k_{1\text{obs}}$ (530 nm), Fig. S44h†). This comparison indicates that Fe^{IV}O does not derive from Fe^{III}(OOH) upon homolytic O–O bond cleavage.

Such an activation of H₂O₂ by Fe^{II} complexes to form Fe^{IV}O species has been reported in slightly acidic aqueous medium⁴³ or in the presence of external or preorganized internal bases,^{33,44,45} which act as a proton shuttle. In these instances H₂O₂ binds to Fe^{II} and the base shuttles a proton from the proximal to the distal O atom, generating an H₂O leaving group

and favoring a heterolytic O–O bond cleavage to generate Fe^{IV}O (Table 1). This process competes with the usual sequence of (i) Fe^{II} oxidation to Fe^{III}(OH); (ii) formation of Fe^{III}(OOH) and H₂O *via* OH/H₂O₂ substitution.

In order to confirm the heterolytic O–O cleavage scenario, we carried out in depth kinetic studies. Eyring plot analysis for the formation of Fe^{IV}O using 2 equiv. H₂O₂ (Fig. S45†) gives activation parameters $\Delta H_{1\text{obs}}^\ddagger = 28 \pm 2 \text{ kJ mol}^{-1}$; $\Delta S_{1\text{obs}}^\ddagger = -144 \pm 5 \text{ J K}^{-1} \text{ mol}^{-1}$ in line with those reported for the heterolytic activation of H₂O₂ by Fe^{II} complexes to form Fe^{IV}O species (Table 1).^{43–45} By comparison, the parameters obtained for the generation of Fe^{IV}O (alongside HO[•]) by homolytic cleavage of the O–O bond of Fe^{III}OOH species are very different.

In the absence of the 2nd sphere phenol moiety (with the parent $[(L_5)\text{Fe}^{\text{II}}(\text{OTf})](\text{OTf})$, Fig. S46†), no such Fe^{IV}O formation is observed, as testified by the absence of 730 nm chromophore upon reaction with H₂O₂. This suggests that the 2nd sphere phenol group must be involved in the heterolytic H₂O₂ activation into Fe^{IV}O. Given the spatial constraints of the ligand backbone, this process would have to be assisted by a water molecule in the case of an intramolecular process, or alternatively, the activation process could be intermolecular. However, the latter hypothesis can be discarded as the growth of the Fe^{IV}O is fitted to a mono-exponential law, in line with an intramolecular process.

To further support this mechanistic proposition, we carried out stopped flow experiments in the presence of additional H₂O/D₂O using MeCN/H₂O 96 : 4 (v/v) as solvent instead of neat MeCN. Interestingly, using D₂O instead of H₂O slightly lowers the Fe^{IV}O rate of formation (Fig. S47†). The kinetic isotope effect (KIE = $k_{1\text{obs}}(\text{H}_2\text{O})/k_{1\text{obs}}(\text{D}_2\text{O})$) determined under these conditions is 1.4 (Fig. S48 and Table S2†). By comparison, among examples of Fe^{II} to Fe^{IV}O conversion assisted by a base, KIE values of 3.7 (ref. 44) and 5.6 (ref. 45) were observed.

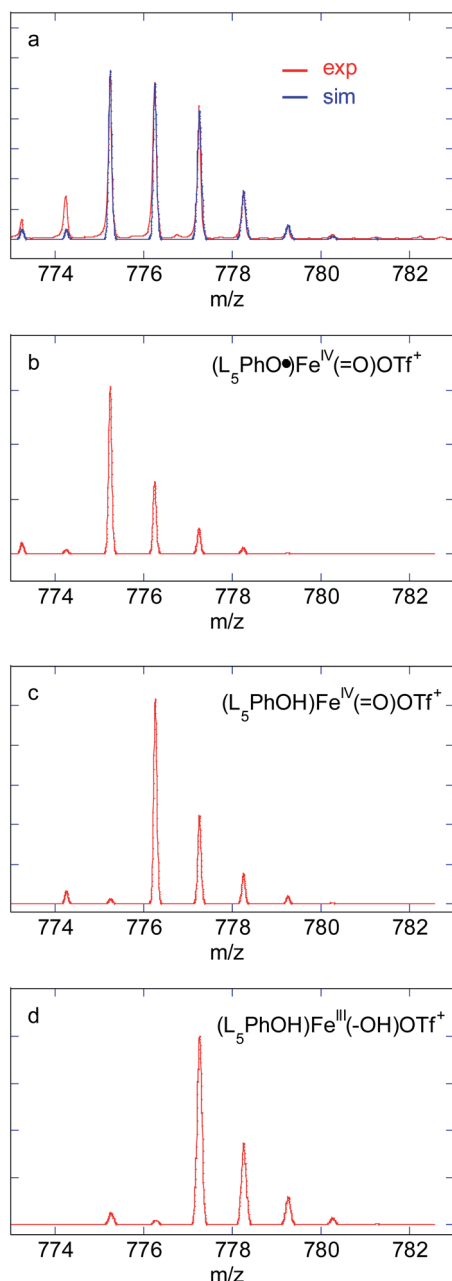


Fig. 4 HR-ESI-MS spectrum (red) recorded upon mixing $[(L_5^{PhOH})Fe^{II}(OTf)](OTf)$ in MeCN with 2 equiv. H_2O_2 at 293 K. Summed simulation (a, blue), isolated simulations: $[(L_5^{PhO})Fe^{IV}(O)(OTf)]^+$: 775.2421 (b), $[(L_5^{PhOH})Fe^{IV}(O)(OTf)]^+$: 776.2499 (c), $[(L_5^{PhOH})Fe^{III}(OH)(OTf)]^+$: 777.2572 (d).

All of these observations point to a fast heterolytic cleavage of H_2O_2 by the Fe^{II} complex which requires the assistance of the surrounding phenol moiety. It can be rationalized using pathway B (Scheme 2): $Fe^{II}(H_2O_2)$ is activated by protonation *via* a network of hydrogen bonds between the distal O atom of the adduct and the phenol moiety likely assisted by water molecules as proton relays. The H_2O/D_2O normal kinetic effect (KIE = 1.4) suggests the cleavage of a O–H(D) bond in the rate determining step of $Fe^{IV}O$ formation. Pathway B (Scheme 2) supports this KIE value as it proposes a PhO–H(D) bond cleavage assisted by

H_2O/D_2O in a Grotthuss-type mechanism. The same trend was already reported for model systems displaying an $Fe^{II}(H_2O_2)$ to $Fe^{IV}O$ conversion.^{44,45}

Decay of $Fe^{IV}O$ generated at low H_2O_2 loading. At low $[H_2O_2]$ (2 equiv. *vs.* Fe, Fig. S35†), $Fe^{IV}O$ is the predominant intermediate, and upon decay, new bands appear at 466 nm, 508 nm and 693 nm. By comparison, these chromophores are not observed after decay of $Fe^{III}(OOH)$ formed at high $[H_2O_2]$ (100 equiv. *vs.* Fe, Fig. S35†). In addition, these bands are clearly different to those the $Fe^{III}(OPh)$ species formed from the $Fe^{IV}O$ generated from PhIO (Fig. 2d) indicating that the fate of this species is dependent on the conditions of its formation. The final bands observed when 2 equiv. H_2O_2 are used are highly reminiscent of oxo-bridged dimeric species reported with N_4 ligand complexes.^{46,47} EPR analysis of the reaction mixture obtained by mixing 2 equiv. H_2O_2 with 4 at 293 K followed by immediate freezing shows very weak signals in the low spin region, in line with an EPR-silent $Fe^{IV}O$ and antiferromagnetically coupled Fe^{III} dimers (Fig. S49 and S50†). The residual signal (Fig. 3d and S50†) consists of $(N_5)Fe^{III}(OH)^{2+}$ ($g = 2.34, 2.140, 1.928$), and $(N_4)Fe^{III}(OOH)(MeCN)^{2+}$ species ($g = 2.205, 2.165, 1.965$)²⁰ together with a small amount of a radical species ($g = 2.004$, presumably phenoxyl radical).

The time evolution of the EPR signal shows a monotonic decrease of the low spin signal, while the high spin signal increases in a first step and decreases in the next (Fig. S51a–d†). This is in line with $Fe^{IV}O$ decaying to give a high spin Fe^{III} complex, which then dimerizes. The double integration of the signal remains low throughout the process when compared to the high H_2O_2 loading (Fig. S51e–g†).

In this experiment (2 equiv. H_2O_2 *vs.* Fe^{II}), the accumulation of $Fe^{IV}O$ is only *ca.* 20% (based on the 730 nm absorbance) and thus a significant amount of H_2O_2 (formally, 9 equiv. *vs.* $Fe^{IV}O$) and Fe^{II} remains in solution: the latter can be seen from the remaining intensity of the $Fe^{II} \rightarrow \pi$ MLCT at low wavelength, at the apex of $Fe^{IV}O$ (Fig. S52†).

The decay rate k_{2obs} (730 nm) increases linearly with $[H_2O_2]$ up to 50 equiv. *vs.* Fe^{II} (Fig. S44g†).⁵⁰ This observation strongly suggests that $Fe^{IV}O$ essentially decays *via* a reaction with H_2O_2 , in agreement with previously reported results.^{33,41,42} The slope gives an estimate of the 2nd order rate $k_2 = k_{2obs}/[H_2O_2] = 77 \text{ L mol}^{-1} \text{ s}^{-1}$, which is much larger than the bimolecular decay rate (reaction with phenol) discussed above ($k = 7.8 \text{ L mol}^{-1} \text{ s}^{-1}$, Fig. S24†). Eqn (1) could rationalize the $[H_2O_2]$ dependence of the $Fe^{IV}O$ decay rate.



The resulting $Fe^{III}(OH)$ could then dimerize to give oxo-bridged EPR-silent species (2), while the second product of reaction (1), HO_2 , could then react with remaining Fe^{II} to generate $Fe^{III}(OOH)$ (3), disproportionate (4), or react with a 2nd $Fe^{IV}O$ species leading $Fe^{III}(OH)$ and O_2 , as already reported (5).⁴²

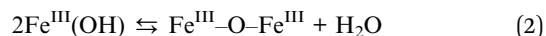
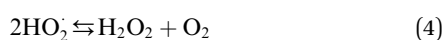


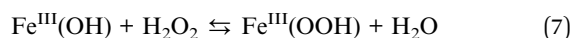
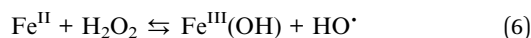
Table 1 Activation parameters for the Fe^{II} to Fe^{IV}O conversion using H₂O₂ by different non-heme Fe^{II} complexes following heterolytic or homolytic O–O cleavage

O–O cleavage	System	ΔH^\ddagger kJ mol ⁻¹	ΔS^\ddagger J mol ⁻¹ K ⁻¹
This work Heterolytic Fe ^{II} → Fe ^{IV} O	[(L ₅ ^{PhOH})Fe ^{II} (OTf)](OTf) + 2H ₂ O ₂ in MeCN	28 ± 2	-144 ± 5
	[Fe ^{II} (^{NH} Bn-tpen)] ²⁺ + H ₂ O ₂ in MeOH ⁴⁵	16	-180
	[Fe ^{II} (L ₅ ²⁺)] ²⁺ + H ₂ O ₂ + NEt ₃ in MeOH ³³	16	-156
	[Fe ^{II} (bispidine ^{N5})] ²⁺ + H ₂ O ₂ in water ⁴³	34	-150
	[Fe ^{II} (TMC)] ²⁺ + H ₂ O ₂ + 2,6-lutidine in MeCN ⁴⁴	29	-144
Homolytic Fe ^{III} (OOH) → Fe ^{IV} O + (HO [•])	[Fe ^{III} (OOH)(L ₅ ²⁺)] ²⁺ (ref. 14)	81	-1
	[Fe ^{III} (OOH)(bppc)] ²⁺ (ref. 48)	53	-68
	[Fe ^{III} (OOH)(TMC)] ²⁺ (ref. 49)	56	-75
	[Fe ^{III} (OOH)(N ₄ Py)] ²⁺ (ref. 49)	53	-121



This set of reactions is in line with the LS residual signals observed by EPR (Fe^{III}(OH) and Fe^{III}(OOH)) and with the final signature in UV-vis spectroscopy (Fe^{III}–O–Fe^{III}). It also fits with the time evolution of the double integration of the EPR signals during Fe^{IV}O decay which remains very weak throughout the process and finally decreases when no H₂O₂ remains and reaction (2) becomes predominant (Fig. S51†).

In the presence of excess H₂O₂, Fe^{III}(OOH) can be formed *via* reactions (6) and (7):



but Fe^{IV}O (which forms faster) can also be converted to Fe^{III}(OH) by the above-mentioned reaction (1), and then to Fe^{III}(OOH) by H₂O₂ substitution (7). In that case, only Fe^{III}(OOH) is accumulated because reaction (7) prevails over reaction (2) due to the excess of H₂O₂.

Discussion

The heterolytic activation of H₂O₂ by non porphyrinic Fe^{II} model complexes is rather scarce. Reported examples involve the addition of an exogenous base,⁴⁴ the role of which is to shuttle the proton from the proximal to the distal O atom in the Fe^{II}/H₂O₂ adduct. A similar activation was reported in slightly acidic conditions, with H₂O likely playing the role of the proton shuttle.⁴³

Incorporation of a base within the complex scaffold has been shown to greatly enhance the selectivity in favor of the quantitative formation of Fe^{IV}O.⁴⁵ Conversely, with a complex displaying the same 1st coordination sphere, with an analogous but exogenous base, a clear competition is observed between the formation of Fe^{IV}O and Fe^{III}(OOH), evidencing the role of preorganization of the 2nd sphere.³³

In using [(L₅^{PhOH})Fe^{II}(OTf)](OTf), a weakly acidic group is incorporated in the 2nd coordination sphere (pK_a of standard phenol is 29.1 in MeCN³¹). The activation parameters derived

from kinetic studies (Eyring plots) indicate a Fe^{IV}O formation mechanism similar to that reported for the above mentioned examples: the distal O atom of the Fe^{II}/H₂O₂ adduct is protonated by the phenol in the rate determining step. Kinetic studies performed in the presence of H₂O or D₂O are also in agreement with this process. However, the phenol moiety is located too far in the ligand backbone to directly protonate the distal O atom of the adduct. Water molecules are likely to act as a relay between them.

The behavior of this complex can be compared to that of its counterpart lacking the phenol group, [(L₅)Fe^{II}(OTf)](OTf). In this latter case, no Fe^{IV}O species is detected upon H₂O₂ addition, only Fe^{III}(OOH) forms and the mechanism was proposed to be described by eqn (6) and (7).²⁰

Together, these data support a mechanism analogous to that described for the heterolytic activation of H₂O₂ by Fe^{II} complexes to form Fe^{IV}O species (Table 1).^{43–45}

Conclusion

We report a new ligand L₅^{PhOH} and its Fe^{II} complexes. In MeCN, complex [(L₅^{PhOH})Fe^{II}(OTf)](OTf) displays a structure with the ligand bound in a pentadentate fashion and the phenol group unbound as a 2nd coordination sphere, as in the structure of complex [(L₅^{PhOH})Fe^{II}Cl](PF₆).

A Fe^{IV}O species is generated with PhIO, and quickly decays by reacting with the dangling phenol group. In reactions involving large amounts of H₂O₂ (100 equiv.), a Fe^{III}(OOH) species is generated, similarly to parent complex missing the phenol [(L₅)Fe^{II}(OTf)](OTf). However, a different behavior between the two complexes is observed at low H₂O₂ concentration. For [(L₅^{PhOH})Fe^{II}(OTf)](OTf), an Fe^{IV}O species is formed predominantly, which is not observed for [(L₅)Fe^{II}(OTf)](OTf). This is ascribed to a “pull” mechanism induced by the acidic 2nd sphere phenol, which favors a heterolytic O–O bond cleavage of H₂O₂ and a direct Fe^{II} to Fe^{IV}O conversion. This activation is supported by the activation parameters of the process and kinetic isotope effects in the presence of H₂O/D₂O.

Author contributions

JNR and FB designed the research, JNR, CH, KSD, RG, TI and HM performed the experimental work, JNR analyzed the data, JNR and FB wrote the paper.

Conflicts of interest

There are no conflicts to declare.

Acknowledgements

This work is supported by a public grant overseen by the French National Research Agency (ANR) as part of the “Investissements d’Avenir” program (Labex charmmmat, reference: ANR-11-LABX-0039-grant).

Notes and references

- 1 I. Bertini, A. Sigel and H. Sigel, *Handbook of metalloproteins*, Marcel Dekker, Inc, New York, 2001.
- 2 I. G. Denisov, T. M. Makris, S. G. Sligar and I. Schlichting, *Chem. Rev.*, 2005, **105**, 2253–2277.
- 3 B. Meunier, S. P. de Visser and S. Shaik, *Chem. Rev.*, 2004, **104**, 3947–3980.
- 4 P. R. Ortiz de Montellano, *Chem. Rev.*, 2010, **110**, 932–948.
- 5 M. Sono, M. P. Roach, E. D. Coulter and J. H. Dawson, *Chem. Rev.*, 1996, **96**, 2841–2888.
- 6 T. L. Poulos, *Chem. Rev.*, 2014, **114**, 3919–3962.
- 7 I. Bertini, H. B. Gray, E. I. Stiefel and J. S. Valentine, *Biological Inorganic Chemistry, Structure and Reactivity*, University Science Books, Sausalito, CA, 2007.
- 8 M. Costas, M. P. Mehn, M. P. Jensen and L. Que, *Chem. Rev.*, 2004, **104**, 939–986.
- 9 S. M. Resnick, K. Lee and D. T. Gibson, *J. Ind. Microbiol. Biotechnol.*, 1996, **17**, 438–457.
- 10 E. Carredano, A. Karlsson, B. Kauppi, D. Choudhury, R. E. Parales, J. V. Parales, K. Lee, D. T. Gibson, H. Eklund and S. Ramaswamy, *J. Mol. Biol.*, 2000, **296**, 701–712.
- 11 A. Karlsson, J. V. Parales, R. E. Parales, D. T. Gibson, H. Eklund and S. Ramaswamy, *Science*, 2003, **299**, 1039–1042.
- 12 M. D. Wolfe and J. D. Lipscomb, *J. Biol. Chem.*, 2003, **278**, 829–835.
- 13 M. Tarasev and D. P. Ballou, *Biochemistry*, 2005, **44**, 6197–6207.
- 14 A. Thibon, V. Jollet, C. Ribal, K. Sénéchal-David, L. Billon, A. B. Sorokin and F. Banse, *Chem.–Eur. J.*, 2012, **18**, 2715–2724.
- 15 A. Company, L. Gomez, X. Fontrodona, X. Ribas and M. Costas, *Chem.–Eur. J.*, 2008, **14**, 5727–5731.
- 16 K. Chen, M. Costas, J. H. Kim, A. K. Tipton and L. Que, *J. Am. Chem. Soc.*, 2002, **124**, 3026–3035.
- 17 O. Cussó, X. Ribas and M. Costas, *Chem. Commun.*, 2015, **51**, 14285–14298.
- 18 A. S. Faponle, F. Banse and S. P. de Visser, *J. Biol. Inorg. Chem.*, 2016, **21**, 453–462.
- 19 A. S. Faponle, M. G. Quesne, C. V. Sastri, F. Banse and S. P. de Visser, *Chem.–Eur. J.*, 2015, **21**, 1221–1236.
- 20 J.-N. Rebilly, W. Zhang, C. Herrero, H. Dridi, K. Sénéchal-David, R. Guillot and F. Banse, *Chem.–Eur. J.*, 2020, **26**, 659–668.
- 21 K. Chen, M. Costas and L. Que Jr, *J. Chem. Soc., Dalton Trans.*, 2002, 672–679, DOI: 10.1039/B108629D.
- 22 V. Baland, F. Banse, E. Anxolabehere-Mallart, M. Ghiladi, T. A. Mattioli, C. Philouze, G. Blondin and J. J. Girerd, *Inorg. Chem.*, 2003, **42**, 2470–2477.
- 23 S. V. Kryatov, E. V. Rybak-Akimova and S. Schindler, *Chem. Rev.*, 2005, **105**, 2175–2226.
- 24 A. Hazell, C. J. McKenzie, L. P. Nielsen, S. Schindler and M. Weitzer, *J. Chem. Soc., Dalton Trans.*, 2002, 310–317, DOI: 10.1039/B103844N.
- 25 M. R. Bukowski, P. Comba, C. Limberg, M. Merz, L. Que Jr and T. Wistuba, *Angew. Chem., Int. Ed.*, 2004, **43**, 1283–1287.
- 26 H.-P. Hersleth, U. Ryde, P. Rydberg, C. H. Görbitz and K. K. Andersson, *J. Inorg. Biochem.*, 2006, **100**, 460–476.
- 27 C. D. Putnam, A. S. Arvai, Y. Bourne and J. A. Tainer, *J. Mol. Biol.*, 2000, **296**, 295–309.
- 28 P. Vidossich, G. Fiorin, M. Alfonso-Prieto, E. Derat, S. Shaik and C. Rovira, *J. Phys. Chem. B*, 2010, **114**, 5161–5169.
- 29 N. Ségaud, J.-N. Rebilly, K. Sénéchal-David, R. Guillot, L. Billon, J.-P. Baltaze, J. Farjon, O. Reinaud and F. Banse, *Inorg. Chem.*, 2013, **52**, 691–700.
- 30 T. Osako, K. Ohkubo, M. Taki, Y. Tachi, S. Fukuzumi and S. Itoh, *J. Am. Chem. Soc.*, 2003, **125**, 11027–11033.
- 31 O. V. Makhlynets and E. V. Rybak-Akimova, *Chem.–Eur. J.*, 2010, **16**, 13995–14006.
- 32 M. Martinho, F. Banse, J. F. Bartoli, T. A. Mattioli, P. Battioni, O. Horner, S. Bourcier and J. J. Girerd, *Inorg. Chem.*, 2005, **44**, 9592–9596.
- 33 A. Bohn, C. Chinaux-Chaix, K. Cheaib, R. Guillot, C. Herrero, K. Sénéchal-David, J.-N. Rebilly and F. Banse, *Dalton Trans.*, 2019, **48**, 17045–17051.
- 34 R. Mayilmurugan, E. Suresh and M. Palaniandavar, *Inorg. Chem.*, 2007, **46**, 6038–6049.
- 35 J. J. Girerd, F. Banse and A. J. Simaan, *Struct. Bonding*, 2000, **97**, 145.
- 36 M. Martinho, P. Dorlet, E. Riviere, A. Thibon, C. Ribal, F. Banse and J.-J. Girerd, *Chem.–Eur. J.*, 2008, **14**, 3182–3188.
- 37 O. Y. Lyakin, I. Prat, K. P. Bryliakov, M. Costas and E. P. Talsi, *Catal. Commun.*, 2012, **29**, 105–108.
- 38 V. Baland, D. Mathieu, N. Pons-Y-Moll, J. F. Bartoli, F. Banse, P. Battioni, J. J. Girerd and D. Mansuy, *J. Mol. Catal. A: Chem.*, 2004, **215**, 81–87.
- 39 A. Thibon, J.-F. Bartoli, R. Guillot, J. Sainton, M. Martinho, D. Mansuy and F. Banse, *J. Mol. Catal. A: Chem.*, 2008, **287**, 115–120.
- 40 M. Martinho, G. Blain and F. Banse, *Dalton Trans.*, 2010, **39**, 1630–1634.
- 41 J. Chen, A. Draksharapu, D. Angelone, D. Unjaroen, S. K. Padamati, R. Hage, M. Swart, C. Duboc and W. R. Browne, *ACS Catal.*, 2018, **8**, 9665.
- 42 J. J. Braymer, K. P. O’Neill, J.-U. Rohde and M. H. Lim, *Angew. Chem., Int. Ed.*, 2012, **51**, 5376–5380.
- 43 J. Bautz, M. R. Bukowski, M. Kersch, A. Stubna, P. Comba, A. Lienke, E. Munck and L. Que, *Angew. Chem., Int. Ed.*, 2006, **45**, 5681–5684.
- 44 F. Li, J. England and L. Que Jr, *J. Am. Chem. Soc.*, 2010, **132**, 2134–2135.

- 45 K. Cheaib, M. Q. E. Mubarak, K. Sénéchal-David, C. Herrero, R. Guillot, M. Clémancey, J.-M. Latour, S. P. deVisser, J.-P. Mahy, F. Banse and F. Avenier, *Angew. Chem.*, 2019, **131**, 864–868.
- 46 S. Taktak, S. V. Kryatov, T. E. Haas and E. V. Rybak-Akimova, *J. Mol. Catal. A: Chem.*, 2006, **259**, 24–34.
- 47 S. Taktak, S. V. Kryatov and E. V. Rybak-Akimova, *Inorg. Chem.*, 2004, **43**, 7196–7209.
- 48 Q. Zhang and C. R. Goldsmith, *Inorg. Chem.*, 2014, **53**, 5206–5211.
- 49 L. V. Liu, S. Hong, J. Cho, W. Nam and E. I. Solomon, *J. Am. Chem. Soc.*, 2013, **135**, 3286–3299.
- 50 The behaviour at higher H₂O₂ loading is due to the concomitant formation of the Fe^{III}OOH chromophore in large quantities at these concentrations: $k_{2\text{obs}}$ (730 nm) becomes a composite of Fe^{IV}O decay and Fe^{III}OOH formation and is thus not reliable to discuss the fate of Fe^{IV}O. Below 50 mM, the absorption of Fe^{III}OOH at 730 nm can be neglected and $k_{2\text{obs}}$ (730 nm) reflects Fe^{IV}O decay alone.
- 51 E. Raamat, K. Kaupmees, G. Ovsjannikov, A. Trummal, A. Kütt, J. Saame, I. Koppel, I. Kaljurand, L. Lipping, T. Rodima, V. Pihl, I. A. Koppel and I. Leito, *J. Phys. Org. Chem.*, 2013, **26**, 162–170.